Supplementary information for

Trapped Exciton Polariton Condensate by Spatial Confinement in Perovskite Microcavity

Shuai Zhang,[1,2] Jie Chen[1,2,3] Jia Shi,[1,2] Lei Fu,[4] Wenna Du,[1,5] Xinyu Sui,[1,2] Yang Mi,[1] Zhili Jia,[1] Fengjing Liu,[1,2] Jianwei Shi,[1] Xinxian Wu, [1,2] Ning Tang,[4] Qing Zhang[3,6] and Xinfeng Liu[1]*

[1]CAS Key Laboratory of Standardization and Measurement for Nanotechnology, CAS Center for Excellence in Nanoscience, National Center for Nanoscience and Technology, Beijing 100190, P. R. China

[2]University of Chinese Academy of Sciences, Beijing 100049, P. R. China

[3]Department of Materials Science and Engineering, College of Engineering, Peking University, Beijing 100871, P. R. China

[4]State Key Laboratory of Artificial Microstructure and Mesoscopic Physics, School of Physics, Peking University, Beijing 100871, P. R. China

[5]Research center for wideband semiconductor, Peking University, Beijing 100871, P. R. China

[*]Email address: liuxf@nanoctr.cn

Table of Content

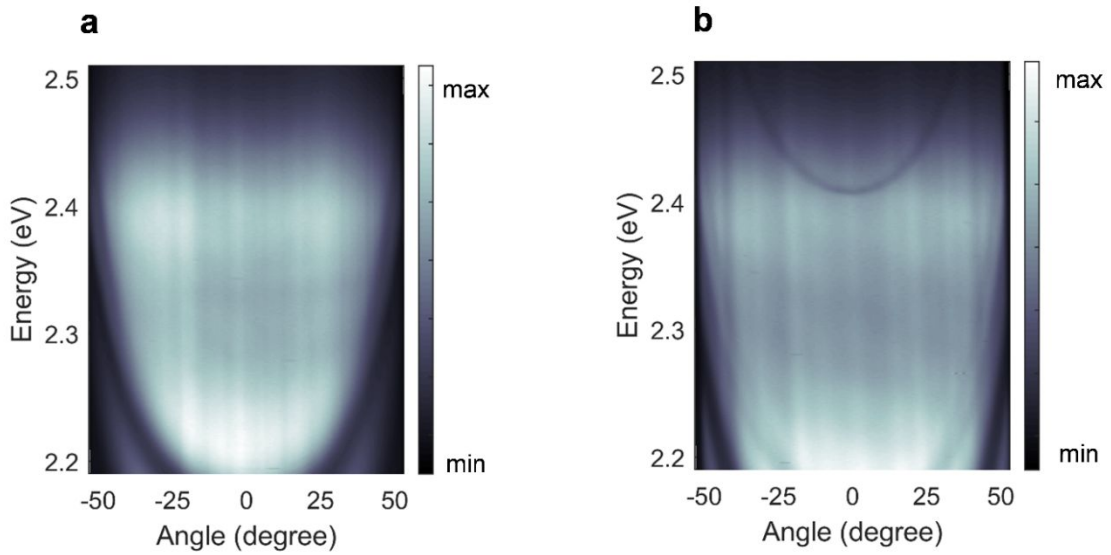

Figure S1 | Photonic Fabry–Pérot mode in empty DBR cavity. (**a**) Before depositing the top layers of DBR, only Bragg modes and optical stop band can be seen in ARR spectral. (**b**) After depositing the top DBR layers without additional filler, a new Fabry–Pérot cavity mode centered at 2.41 eV generates in the gap region.

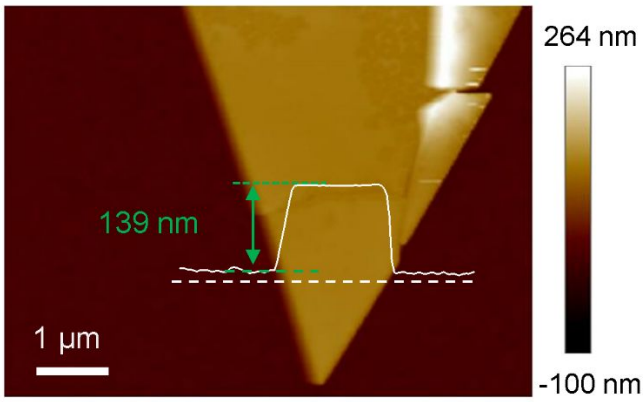

Figure S2 | Atomic force microscopy (AFM) image of a typical $CsPbBr_3$ thin flake with a thickness of 139 nm. The wrinkle results from stress in transfer of sample. Scale bar, 1μm.

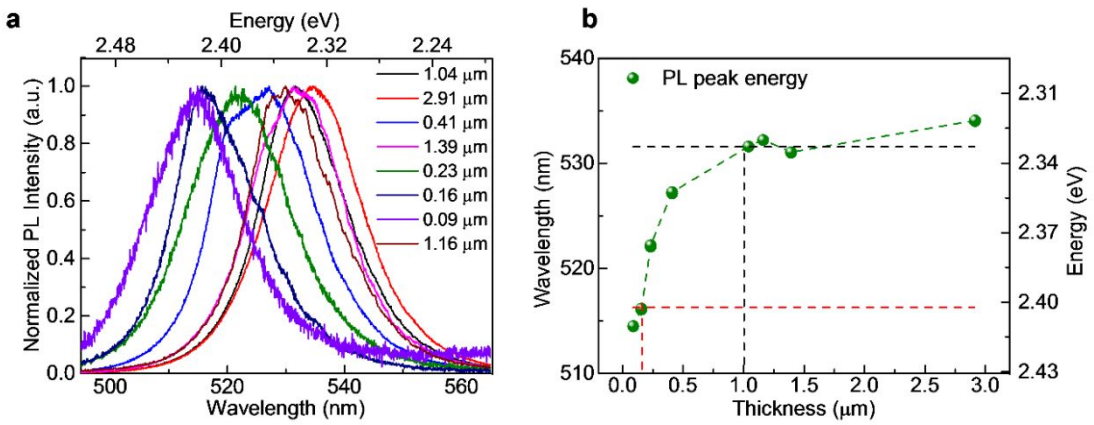

Figure S3 | PL emission of $CsPbBr_3$ flakes with different thickness. (**a**) Normalized PL intensity of $CsPbBr_3$ flakes with different thickness and width of 5-10 μm. The thickness is determined by AFM. (**b**) The PL peak energy (olive dots with dash guided line) versus thickness extracted from (a). The black and red dash line indicates the approximate emission energy of the flakes with thickness of 1 μm and 150 nm.

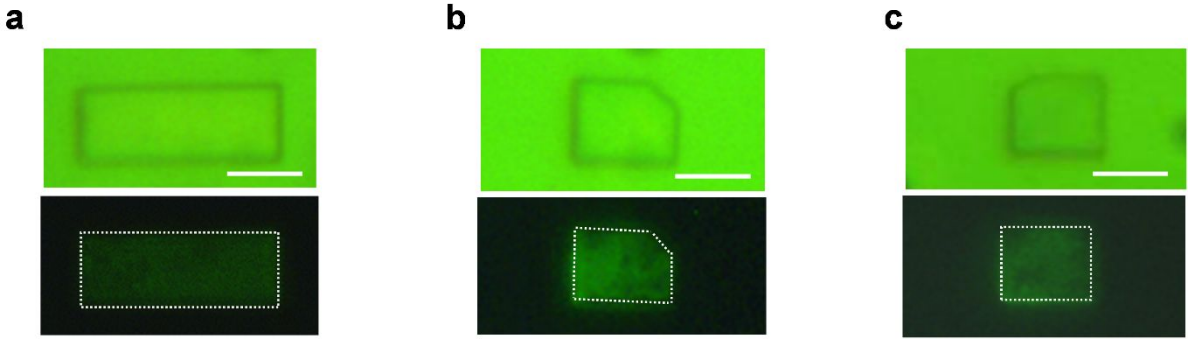

Figure S4 | Real-space images of $CsPbBr_3$ flakes in figure 2. (a-c) are optical images (upper) and corresponding emission images (lower) below threshold of the flakes in figure 2a-c. Scale bar, 5 μm.

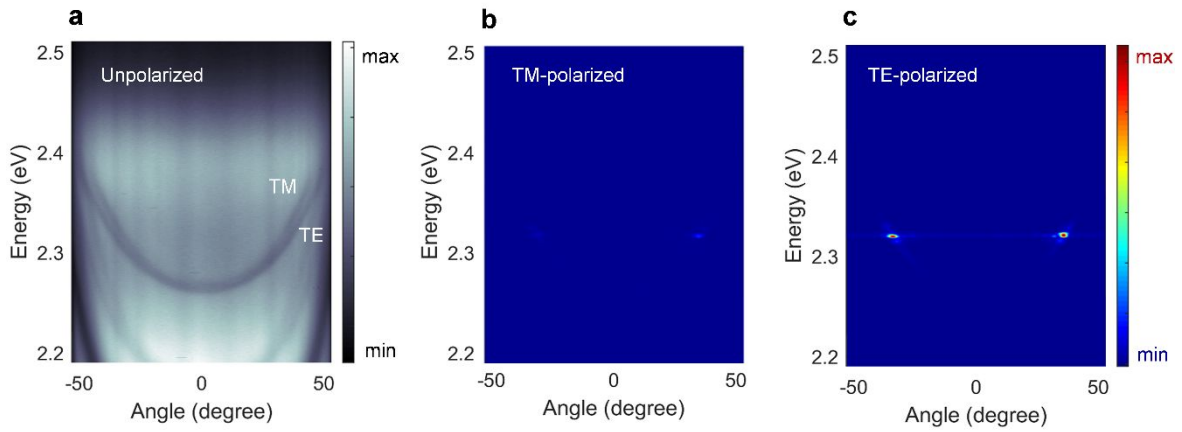

Figure S5 | Polarization of polariton dispersion. (a)TE-TM splitting at large angle in the ARR spectra of the $CsPbBr_3$ flake in **figure 1a,d** with its longer side parallelled to y axis. (b) TM polarized ARE spectra above laser threshold by using a polarizer with vertical polarization before the spectrometer. By changing the polarization to horizontal direction, TE polarized ARE spectra can also be obtained in (c). The intensity in (b) and (c) have been scaled to the maximum intensity of TE- polarized ARE spectra, indicating that polariton emission are more TE like.

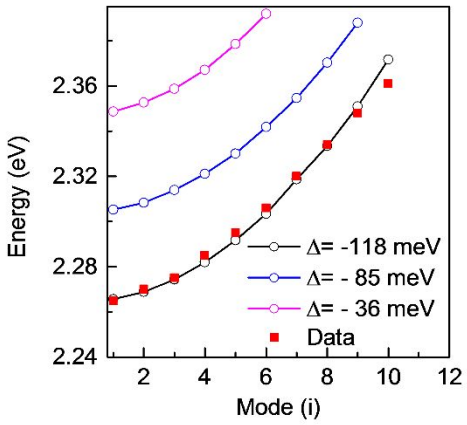

Figure S6 | Calculated discrete polariton energy$E_i$induced by optical trap at different detuning.The red dots are experimental data.

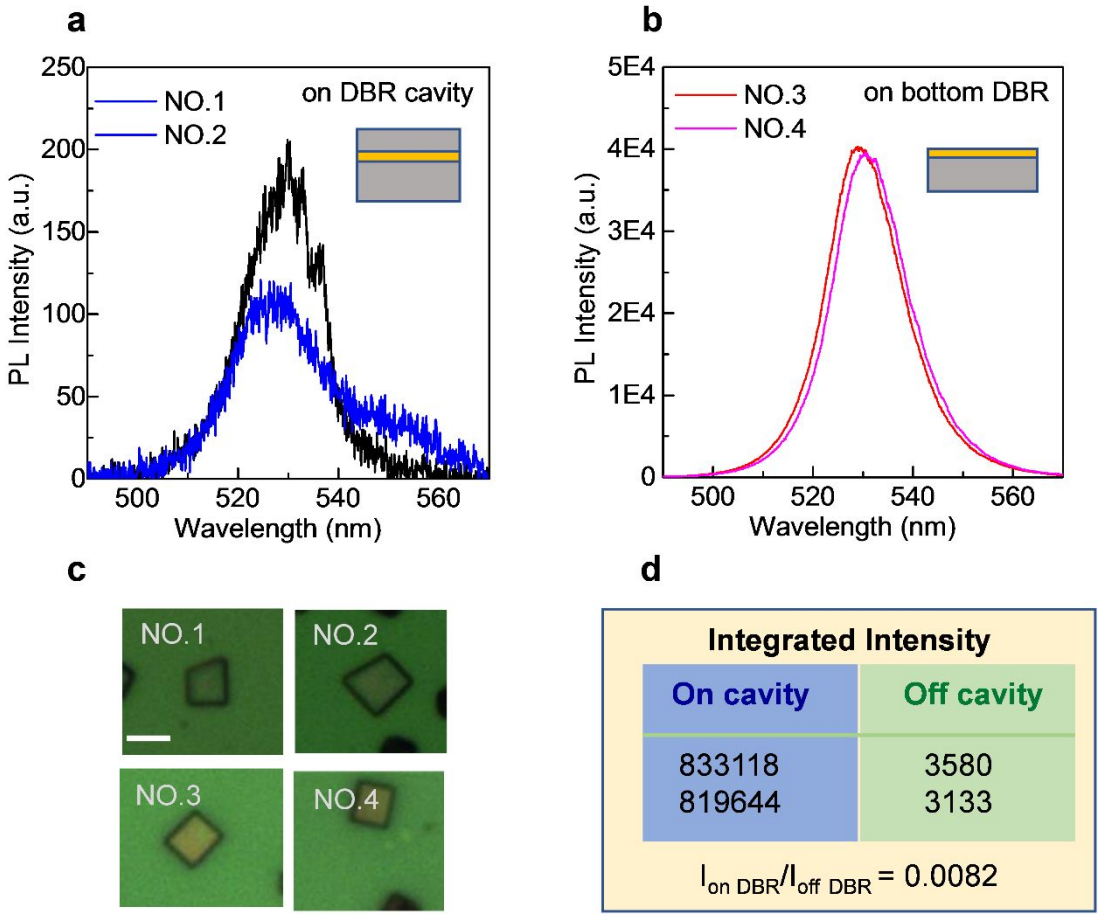

Figure S7 | Estimation of injected laser power inside cavity**.** (**a**) Emission spectral of two perovskite flakes marked as NO.1-2 inserted in the DBR cavity with the intrinsic PL peak of 527-530 nm. (**b**) PL spectral of two perovskite flakes NO.3-4 on the bottom DBR mirror with the same pump power as in (a) and PL peak of 528-530 nm. The similar PL peaks suggest the similar thickness of perovskite flakes. (**c**) Corresponding optical images of perovskite flakes. Scale bar is 10 μm. (**d**) Integrated intensity of samples on cavity (NO. 1-2) and off cavity (NO. 3-4) with the same excitation condition. The ration of this value indicates the rate of laser power transmitted into the cavity.

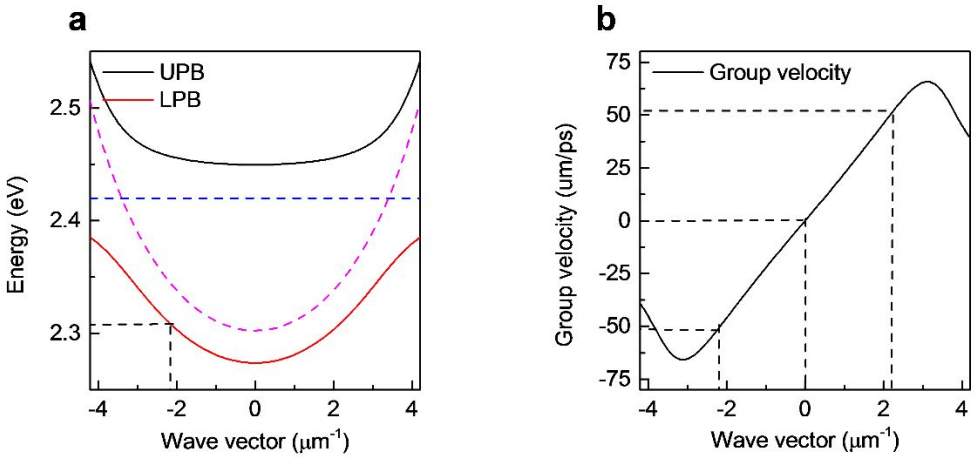

Figure S8 | Group velocity of discrete polariton mode. (a) Polariton dispersion of sample in figure 3 converted to the energy-wave vector ($k_{\parallel}$) coordinates. The blue and pink dash lines are uncoupled exciton resonant energy and cavity mode. The black dash line indicates the coordinate of the first polariton condensed mode E_4 shown in figure 3a. (b) Group velocity of the LPB with marked positon of E_4 (±51 μm/ps) and bottom of LPB (0).

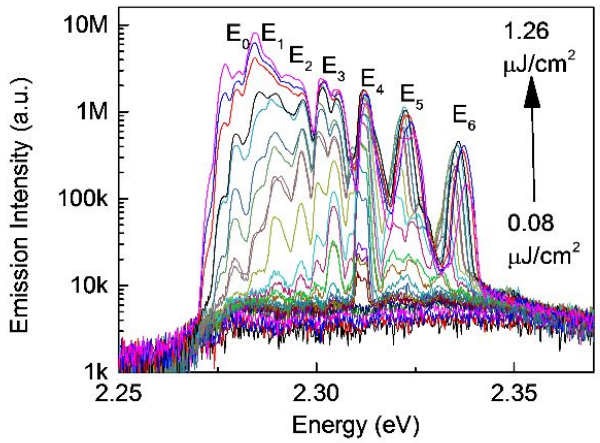

Figure S9 | Emission spectra of the perovskite/DBR microcavity with detuning energy of -118 meV at different pump fluence. E_{0-6} indicate discrete polariton states above laser threshold. At high pump fluence, E_{0-2} are mixed together.

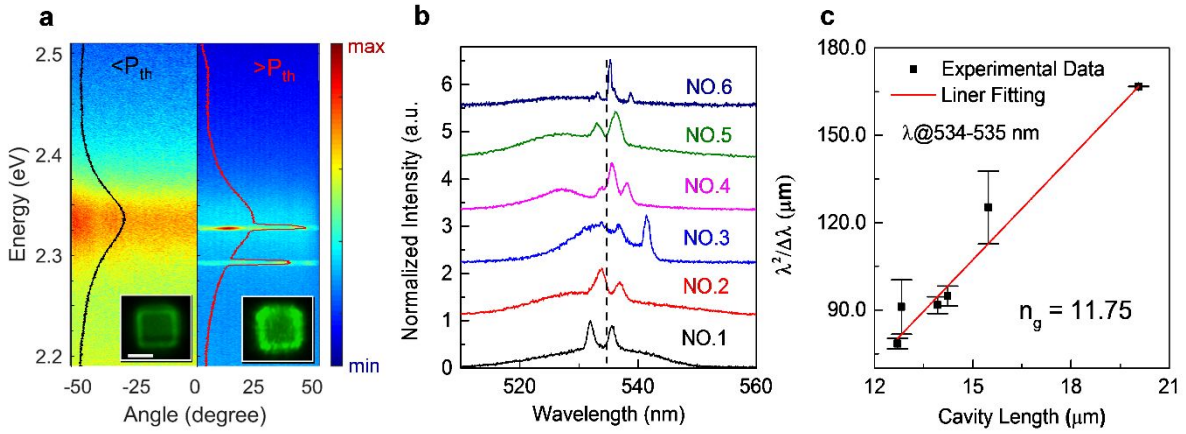

Figure S10 | WGM mode laser in $CsPbBr_3$ bulk square crystals inside the DBR cavity. (a) ARE spectral of the cavity with the perovskite thickness of ~500 nm. Left part, below threshold, corresponds to spontaneous emission. Right part, above threshold, corresponds to laser behavior. The red solid lines are the emission spectral at the same energy coordinate. Inserts at the bottom are optical images at corresponding pump fluence. Scale bar, 2 μm. (b) Normalized emission spectra above laser threshold for six bulk samples. The black dash line indicates the wavelength where group index n_g is to be analyzed. (c) The value of $\lambda^2/\Delta\lambda$ (black dots) versus cavity length L at the fixed wavelength of 534.7 nm is fitted by the relation $\lambda^2/\Delta\lambda = n_g/L$.[1] The cavity length of WGM cavity can be expressed as $L = 2\sqrt{2}d$ where d is the edge length of a square cavity.

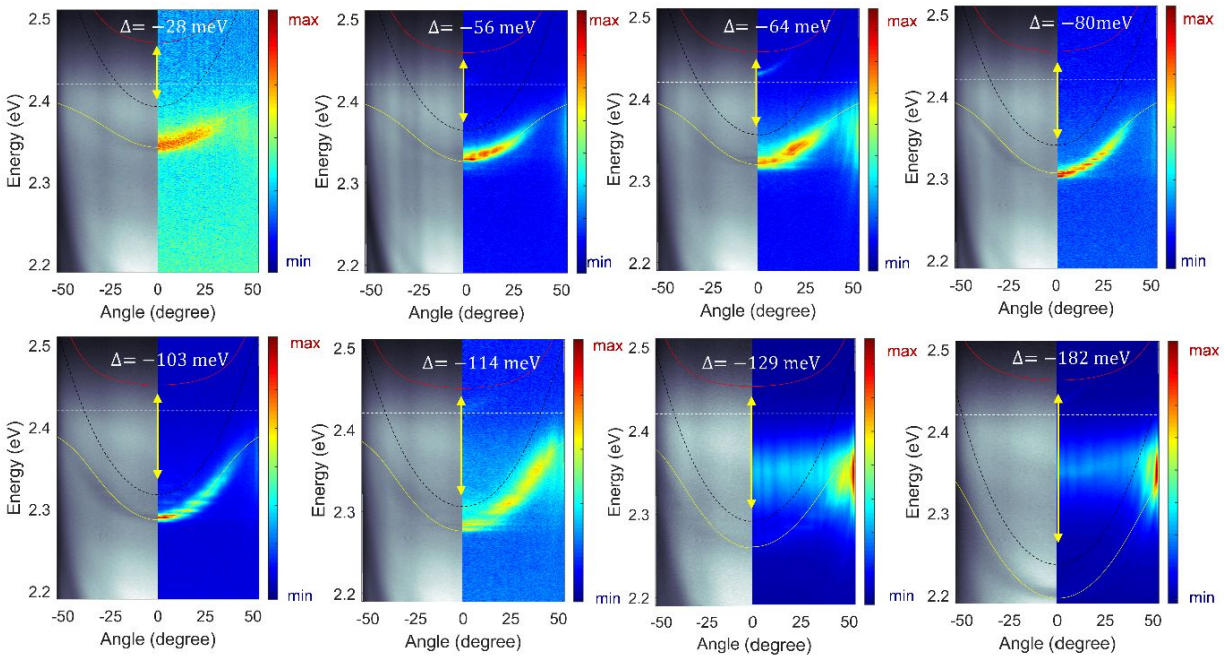

Figure S11 | Angle-resolved reflectivity (left part) and angle-resolved emission (right part) of perovskites at different detuning energies from -28 meV to -182 meV. The yellow arrows indicate the energy difference of cavity mode and exciton energy.

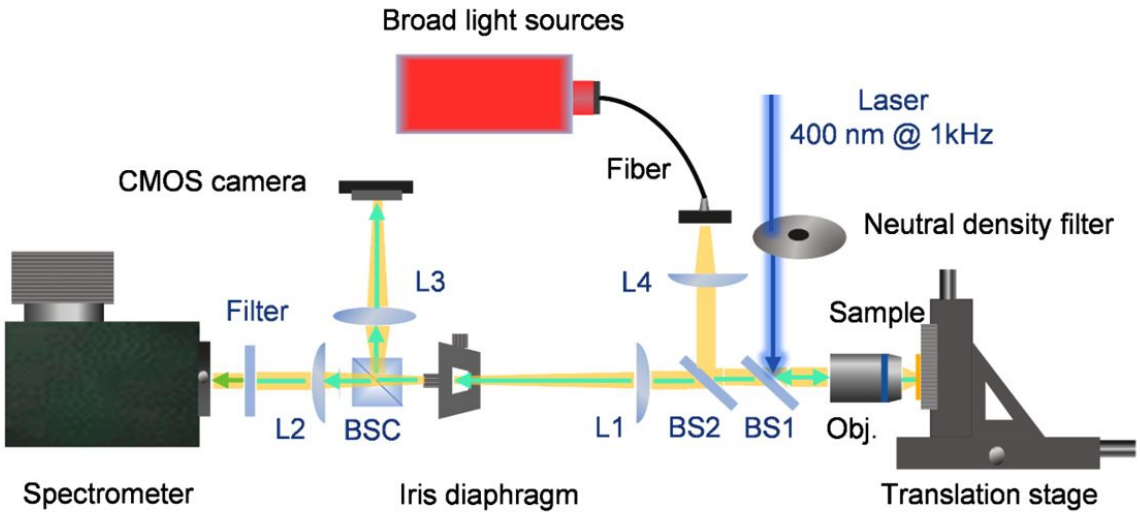

Figure S12 | Optical setup for angle-resolved spectroscopy by spatially-resolved Fourier imaging. BS1 and BS2 are beam splitters for introducing laser source and white light. Obj. is a 50× objective lens. L1, L2 and L3 are lenses for transformation between real-space image and Fourier image. L4 is a lens for collimation of white light. BSC is the beam-splitter cube for the observation of Fourier image and corresponding real-space image simultaneously.

Note S1: Polariton dispersion model in perovskite/DBR cavity

We define the refractive index and thickness of two periodic layers of the DBR mirrors as n_1, n_2 and L_1, L_2. The cavity mode dispersion can be expressed as[2]

$$E_c(\theta) = \left(E_S(\theta)L_S + E_P(\theta)L_P(\theta)\right)/L_{eff}(\theta) \quad \text{(S1)},$$

Here L_S and L_P are cavity space between two DBRs and penetration depth into two DBRs, and the effective cavity length $L_{eff} = L_S + L_P$. $E_S(\theta)$ and $E_P(\theta)$ are Fabry-Pe´rot energy considering no phase delay in the mirrors and center of the stop band energy. They are expressed as:

$$E_S(\theta) = m\pi\hbar c/n_{cav}L_S\cos(\theta_S),\ E_P(\theta) = \frac{\hbar\pi c}{2(L_1 + L_2)}\frac{n_1\cos\theta_1 + n_2\cos\theta_2}{n_1 n_2\cos\theta_1\cos\theta_2} \quad \text{(S2)},$$

where m is the mode order, n_{cav} is the refractive index of the intracavity region. For a light emitted from the cavity with a certain angle θ, θ_S and θ_{1-2} are the incident angles inside the active layer and two periodic layers, which can be determined by transfer matrix approach.[3]

The dispersion of exciton-polariton is modeled by coupled oscillator containing the excitonic energy E_x and cavity mode $E_c(\theta)$ as

$$\begin{pmatrix} E_x(\theta) - i\hbar\gamma_x & V \\ V & E_c(\theta) - i\hbar\gamma_c \end{pmatrix}\begin{pmatrix} c_x \\ c_c \end{pmatrix} = E_p(\theta)\begin{pmatrix} c_x \\ c_c \end{pmatrix} \quad \text{(S3)}$$

where γ_x and γ_c are the linewidth of exciton and cavity photon, V is the coupling strength. c_x and c_c are Hopfield coefficients for describing the relative proportion of exciton and photon with the relation of $c_x^2 + c_c^2 = 1$.

The resulted two polariton branches are

$$E_{UP,LP} = \frac{1}{2}\left[E_X + E_c(\theta) + i(\gamma_c + \gamma_X) \pm \sqrt{4V^2 + E_X - E_c(\theta) + i(\gamma_c - \gamma_X)^2}\ \right] \quad \text{(S4)}.$$

Here we use the parameter of angle θ obtained by angle-resolved spectroscopy which can be equivalent to the in-plane wave vector $k_{\parallel} = \frac{m\pi}{n_{cav}L}tan\left[sin^{-1}\left(\frac{sin\theta}{n_{cav}}\right)\right]$, where m is the mode order, L is cavity length.

Note S2: fitting parameters of polariton model

The dielectric function of $CsPbBr_3$ is adopted from the report of Eaton, S. W. *et.al.*[4] Excitonic energy $E_X = 2.42$ eV and linewidth of $\hbar\gamma_X = 73.6\ meV$ is obtained from the intrinsic PL and absorption spectral. Linewidth of VFPC mode (embedded with perovskite flakes) is deduced from the fitting of polariton linewidth of LPB at different angles by[5-6]

$$\gamma_{LP} = |c_x|^2\gamma_x + |c_c|^2\gamma_c \qquad \text{(S5)}.$$

Hopfield coefficients c_x and c_c of LPB is expressed as:

$$c_x = -\sqrt{\frac{1}{2} + \frac{\Delta(\theta)}{2\delta(\theta)}}, \quad c_c = \sqrt{\frac{1}{2} - \frac{\Delta(\theta)}{2\delta(\theta)}} \qquad \text{(S6)},$$

where $\delta(\theta) = \sqrt{\Delta(\theta)^2 + 4V^2}$ and $\Delta(\theta) = \sqrt{E_c(\theta) - E_X}$ is the detuning energy. To obtain the linewidth of cavity mode, we analyzed the emission spectral at different angle from the ARE spectral with the detuning of -139 meV in **figure S12(a)**. The linewidth of polariton by simulation and emission spectral are displayed in **figure S12 (b)** with the fitted value of $\hbar\gamma_c$ = 10 meV. The experimental values at large angle may have large deviation due to the disturbing intrinsic emission of perovskite.

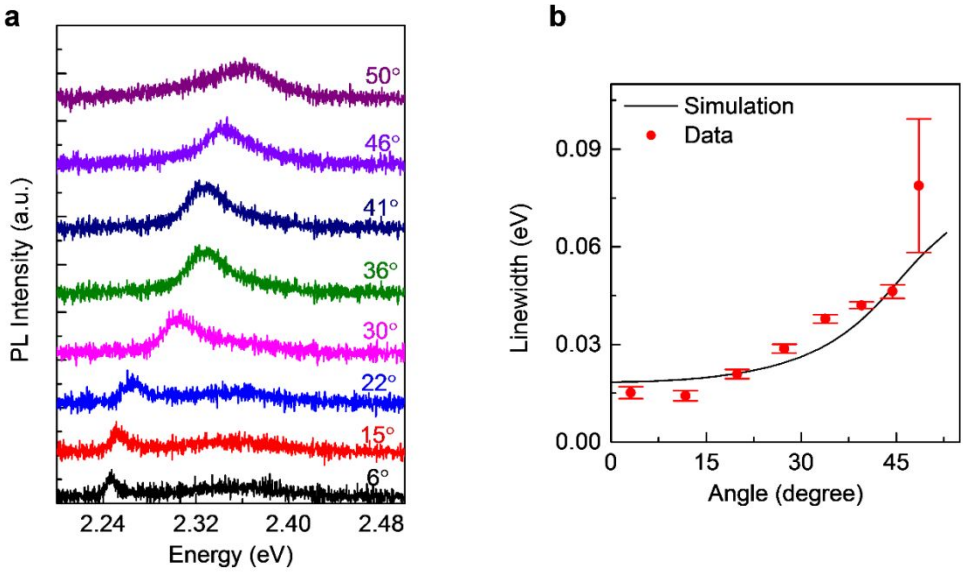

Figure S13 | Fitting of the polariton linewidth. **(a)** Emission spectral of perovskite/DBR microcavity at different angle with the detuning of -139 meV. (b) Polariton linewidth fitted from emission spectral (red dots) and simulation result (black line) using the equation (S3).

Note S3: Simulation of rate equations for kinetic model

To simulate the rate equations (2-3) in main text, we should obtain the lifetime of exciton in reservoir and polaritons at different energies. The polariton's lifetimes $\tau_p$can be determined by the relation below:

$$\frac{1}{\tau_p} = \frac{c_c^2}{\tau_c} + \frac{c_x^2}{\tau_x} \qquad \text{(S7)}.$$

Hopfield coefficients c_c and c_x can be obtained from the dispersion model. The value of cavity mode lifetime $\tau_c = {}^{Q}/_{\omega_c}$, and the quality factor $Q = {}^{E_c}/_{FWHM}$ can be obtained by using $E_c = 2.3\ eV$ and FWHM=10 meV. The lifetime of exciton is measured by testing the photoluminescence (PL) decay of $CsPbBr_3$ flakes on silicon wafer. The lifetime of exciton and polariton at different energies are shown in **Figure S14**.

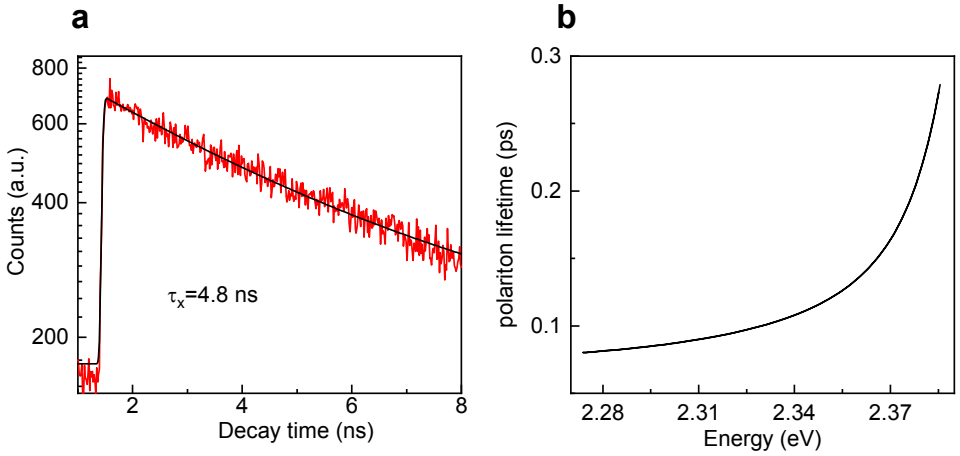

Figure S14 | Lifetime of exciton and polariton at different energies of LPB. (a) PL decay of $CsPbBr_3$ flake. The decay $I(t)$ can be fitted by a single exponential decay relation $I(t) = I_0 + A \cdot \exp(-t/\tau)$ with fitted value of τ=4.8 ns. (b) Calculated polariton lifetime at different energy of LPB by using the relation (S7).

The decay rate of exciton Γ_x and polariton at different energy states Γ_i is simply the reciprocal of their lifetimes. However, the energies of E_i are blue shifted with the increasing pump fluence. To simplify the simulation, we trace the peak energies of different polariton states E_i at different pump fluence from **Figure S9** and take the average values as the energy value for simulation. The average energies of different energies are $E_3 = 2.304\ eV$, $E_4 = 2.314\ eV$, $E_5 = 2.323\ eV$. They behave as similar energy spacings and suitable for polariton-polariton scattering. Considering that the intensities of E_{0-2} are difficult to be analyzed separately, we define an overall energy state $E_{0-2} = 2.295\ eV$ for the scattering

between E_{0-2} and higher energy states. Next, the decay rates of exciton in reservoir $\Gamma_x = 1/4800ps^{-1}$ and polaritons at different states $\Gamma_{0-2} = 1/0.084ps^{-1}$, $\Gamma_3 = 1/0.088ps^{-1}$, $\Gamma_4 = 1/0.091ps^{-1}$, and $\Gamma_5 = 1/0.095ps^{-1}$are used. The excitation pulse is expressed as $N = N_0 \cdot \exp\left(-\left(\frac{t-t_0}{\Delta}\right)^2\right)$ with pulse width $\Delta = 0.1\,ps$ and $t_0 = 1ps$. The time-resolved population of different energy sates with the parameters $A = 4 \times 10^{-7}$, $B = 0.01A$, and $N_0 = 1 \times 10^6$ is shown in **Figure S15**

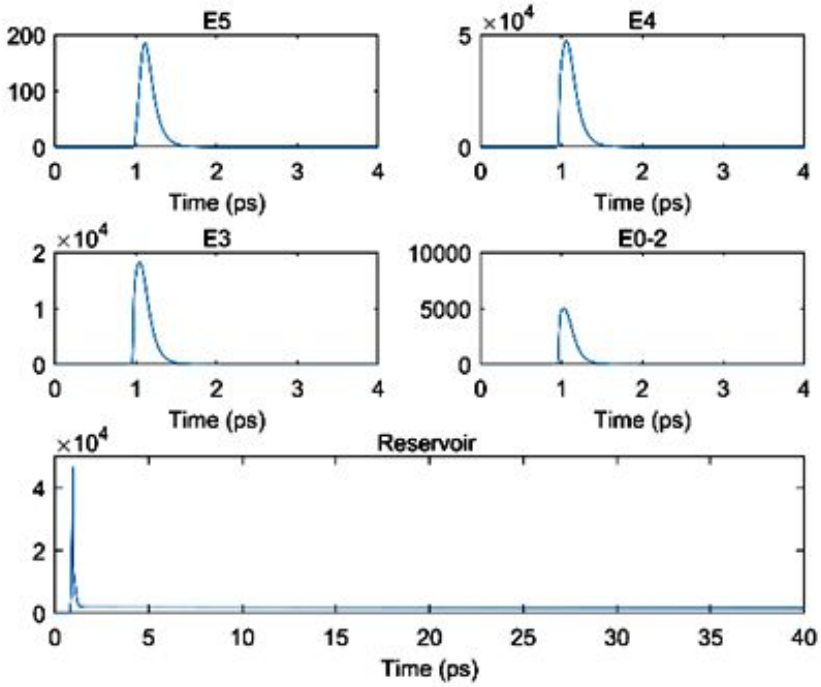

Figure S15 | Time-resolved population distribution of different polariton state and exciton in reservoir at the pumped population of $N_0 = 1 \times 10^6$.

The integrated intensities of different energy states at different pumped population can be obtained by sweeping the population of pumped pulse from 10^6 to 10^9, see **Figure 3e** in main text.

Note S4: Mean-field Gross–Pitaevskii equation of driven-dissipative model

Considering the nonequilibrium polariton condensate generated in a cavity with finite lateral dimension under a homogeneous pumping, a mean-field description of a condensate wave function can be adopted as the generalized Gross–Pitaevskii equation:[7]

$$i\hbar\frac{\partial\psi(r,t)}{\partial t} = \left(E_0 - \frac{\hbar^2}{2m}\nabla_r^2 + \frac{i\hbar}{2}[(R(n_r) - \gamma_p)] + \hbar g_p|\psi(r,t)|^2 + V(r)\right)\psi(r,t) \quad \text{S (8)},$$

Here E_0 and m are the minimum energy and effective mass of the LPB, g_p is the strength of repulsive interaction between condensate polaritons. $R(n_r)$ and γ_p are scattering rate (gain rate) and loss rate of condensate polaritons. $V(r)$ is the external potential including confinement potential $V_{conf}(r)$ defined by the cavity edge under study, and mean-field repulsive potential $V_{res}(r) = \hbar g_X n_r$ induced by interaction between exciton reservoir n_r and polariton. The exciton reservoir can be described by a rate equation:

$$\dot{n_r} = P(t) - \gamma_X n_r - R(n_r)|\psi(r,t)|^2 \quad \text{S (9)},$$

where the exciton reservoir decay rate $\gamma_X \gg \gamma_p$ and depletion of the reservoir due to stimulated scatter into condensate mode are considered.

Considering a rectangular cavity with edge length of L_x and L_y, and effective mass m, the $V_{conf}(r)$ can generate the quantization potential energy $E_{x,y} = \frac{\pi^2\hbar^2}{2m}\left(\frac{n_x^2}{L_x^2} + \frac{n_y^2}{L_y^2}\right)$, which is equivalent to the optical mode energy in such planer cavity. At large negative detuning, the repulsive potential between exciton reservoir and polariton $V_{res}(r)$ is relatively weak, then $V(r) \cong V_{conf}(r)$.[8] These results in the multi-mode polariton both below and above nolinear threshold (see **Figure 3**). In contrast, for a small negative detuning, polaritons are more exciton like with large repulsive potential $V_{res}(r)$. The external potential is more influenced by $V_{res}(r)$, i.e., $V(r) \cong V_{res}(r)$.[9] This can be evidenced as single dispersion curve and stationary condense at zero momentum of LPB E_{st} (see **Figure 4**). Compared to the initial energy of the bottom of LPB E_0, there is a linear bluesified energy depending on the pumping rate P:[7]

$$E_{st} - E_0 = \hbar g_p|\psi(0)|^2 + \hbar g_X n_r = \frac{\hbar g_p}{\hbar\gamma_p}(P - P_{th}) + \frac{\hbar g_x}{\hbar\gamma_x}P_{th} \quad (P > P_{th}) \quad \text{S (10)}$$

$$E_{st} - E_0 = \hbar g_X n_r = \frac{\hbar g_x}{\hbar\gamma_x}P \quad (P < P_{th}) \quad \text{S (11)}$$

Note S5: Finite element simulation of the electronic field of perovskite in DBR cavity

The simulation is based on a three – dimensional FDTD method with perfectly matched layer (PML) boundary conditions and cavity structure shown as below in x-z direction, which is based on the parameter introduced in experimental section. To compare the electronic field of cavity with thin perovskite flake and bulk crystal, we design the cavity structures with perovskite thickness of 150 nm and 1 μm (at z direction) and same width of perovskite (1×0.8 μm in x-y direction) and mirrors (2.5×1.5 μm in x-y direction) shown in **Figure S16**. Different material of the cavities is identified by the refractive index.

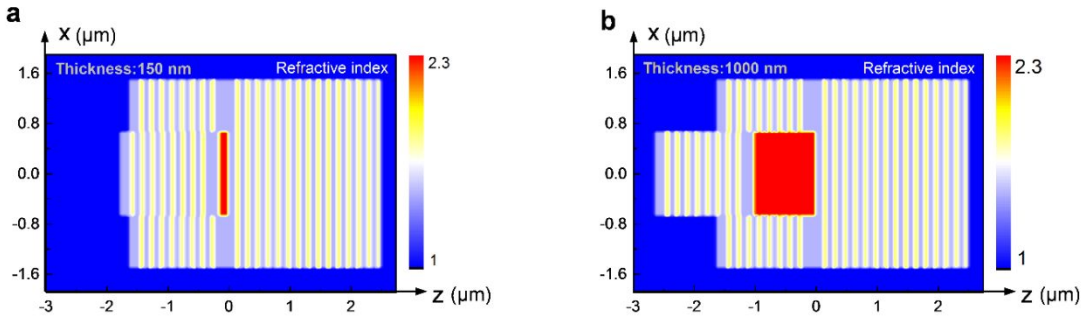

Figure S16 | Cavity structures and refractive index of the simulated model at x-z coordinates. (a) and (b) are cavities with different thickness of perovskite, i.e., 150 nm and 1 μm, respectively.

A transverse electric (TE) - polarized mode source with central wavelength of 516 nm and 530 nm (corresponding to the intrinsic PL peaks at these thicknesses, see **Figure S3**) is introduced in the sandwiched perovskite layer. Electronic field $|E|^2$at x-y coordinates is monitored at 530 nm where cavity emission can be observed in these two cavities. **Figure S17** is the $|E|^2$ of different vector attribution for these two cavities. The intensity of $|\mathrm{E}_i|^2$ at different vectors ($\mathrm{i} = \mathrm{x,y,z}$) have been normalized to the magnitude of $|E|^2$ at all vectors.

In the cavity with perovskite thickness of 150 nm, the electronic field at z vector is more favored at the central of perovskite cavity with amplitude of 0.62, where efficient generation of VFPC modes and coupling with excitons can be expected. For comparison, $|E|^2$ of the 1 μm - thickness is more concentrated on x vector, with slight components at z (0.11) and y vector (not shown here). This suggests the inefficient generation of VFPC modes and hindering the strong coupling between VFPC modes and excitonic emission inside the perovskite crystal. Optical

image also reveals that light leaks out from the crystal edge (see left part of **Figure S10a**), which is in contrast to that in **Figure S4** where the emission below threshold is mainly uniform. Therefore, the photonic laser occurs as the WGM laser rather than from the VFPC optical mode.

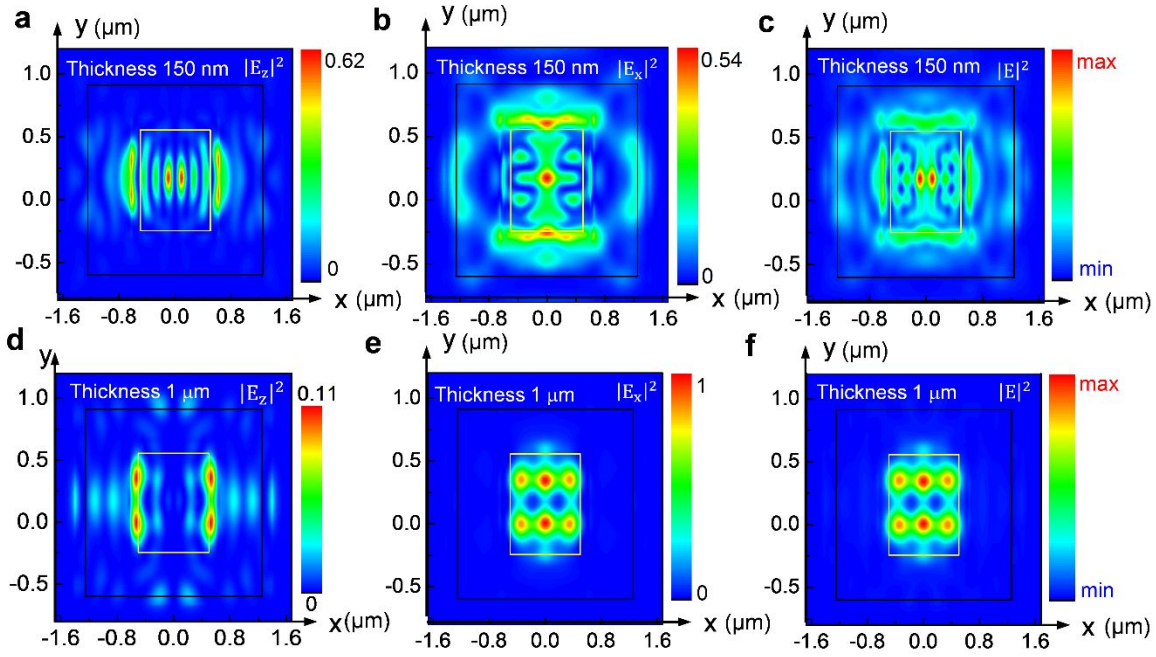

Figure S17 | Distribution of electric field at the cross section of perovskite. (a-c) are the electric field of the cavity with 150 nm perovskite thickness at z vector of $|E_z|^2$, x vector $|E_x|^2$, and magnitude of $|E|^2$, respectively. (d-e) are the electric field of the cavity with the bulk perovskite crystal at z vector $|E_z|^2$, x vector $|E_x|^2$, and magnitude of $|E|^2$.

References:

1. Fang, H.-H.; Ding, R.; Lu, S.-Y.; Yang, Y.-D.; Chen, Q.-D.; Feng, J.; Huang, Y.-Z.; Sun, H.-B., Whispering-gallery mode lasing from patterned molecular single-crystalline microcavity array. *Laser & Photonics Reviews* **2013,** *7*, 281-288.
2. Panzarini, G.; Andreani, L. C.; Armitage, A.; Baxter, D.; Skolnick, M. S.; Astratov, V. N.; Roberts, J. S.; Kavokin, A. V.; Vladimirova, M. R.; Kaliteevski, M. A., Cavity-polariton dispersion and polarization splitting in single and coupled semiconductor microcavities. *Physics of the Solid State* **1999,** *41*, 1223-1238.
3. Citrin, D. S., Material and optical approaches to exciton polaritons in multiple quantum wells: Formal results. *Physical Review B* **1994,** *50*, 5497-5505.
4. Eaton, S. W.; Lai, M.; Gibson, N. A.; Wong, A. B.; Dou, L.; Ma, J.; Wang, L.-W.; Leone, S. R.; Yang, P., Lasing in robust cesium lead halide perovskite nanowires. *Proceedings of the National Academy of Sciences* **2016,** *113*, 1993-1998.
5. Pan, L. D.; Zhang, L. Z.; Song, B. Q.; Du, S. X.; Gao, H.-J., Graphyne- and graphdiyne-based nanoribbons: Density functional theory calculations of electronic structures. *Applied Physics Letters* **2011,** *98*, 173102.

6. Bouteyre, P.; Nguyen, H. S.; Lauret, J.-S.; Allard-Trippé, G.; Delport, G.; Lédée, F.; Diab, H.; Belarouci, A.; Seassal, C.; Garrot, D., Room temperature cavity polaritons with 3D hybrid perovskite-Towards low-cost polaritonic devices. *arXiv preprint arXiv:1810.05720* **2018**.
7. Wouters, M.; Carusotto, I.; Ciuti, C., Spatial and spectral shape of inhomogeneous nonequilibrium exciton-polariton condensates. *Physical Review B* **2008,** *77*, 115340.
8. Sanvitto, D.; Amo, A.; Viña, L.; André, R.; Solnyshkov, D.; Malpuech, G., Exciton-polariton condensation in a natural two-dimensional trap. *Physical Review B* **2009,** *80*, 045301.
9. Wouters, M.; Carusotto, I., Excitations in a Nonequilibrium Bose-Einstein Condensate of Exciton Polaritons. *Physical Review Letters* **2007,** *99*, 140402.